tvst

Article

Laser Capture Microdissection-Based RNA Microsequencing Reveals Optic Nerve Crush-Related Early mRNA Alterations in Retinal Ganglion Cell Layer

Dongyan Pan[1,7,*], Mengqiao Xu[2,8–11,*], Xin Chang[1,*], Mao Xia[3,*], Yibin Fang[4], Yinghua Fu[5], Wei Shen[1], Yue Wang[6,7], and Xiaodong Sun[2,8–11]

[1] Department of Ophthalmology, Changhai Hospital, Second Military Medical University, Shanghai, China
[2] Shanghai General Hospital, Shanghai, China
[3] The 12th Hospital of PLA, China
[4] Department of Neurosurgery, Changhai Hospital, Second Military Medical University, Shanghai, China
[5] College of Optoelectronic Information and Computer Engineering, University of Shanghai for Science and Technology, Shanghai, China
[6] Department of Histology & Embryology, Second Military Medical University, Shanghai, China
[7] Shanghai Key Lab of Cell Engineering, Shanghai, China
[8] National Clinical Research Center for Eye Diseases, Shanghai, China
[9] Shanghai Key Laboratory of Ocular Fundus Diseases, Shanghai, China
[10] Shanghai Engineering Center for Visual Science and Photomedicine, Shanghai, China
[11] Shanghai Engineering Center for Precise Diagnosis and Treatment of Eye Diseases, Shanghai, China

Correspondence: Wei Shen, Department of Ophthalmology, Changhai Hospital, Second Military Medical University, Shanghai, China, 200433. e-mail: shenwzz@163.com Yue Wang, Department of Histology & Embryology, Second Military Medical University, Shanghai, China, 200433. e-mail: wangyuesmmu@163.com

Received: March 25, 2020
Accepted: September 20, 2020
Published: October 27, 2020

Keywords: laser capture microdissection; microsequencing; optic nerve crush; retinal ganglion cell layer

Citation: Pan D, Xu M, Chang X, Xia M, Fang Y, Fu Y, Shen W, Wang Y, Sun X. Laser capture microdissection-based RNA microsequencing reveals optic nerve crush-related early mRNA alterations in retinal ganglion cell layer. Trans Vis Sci Tech. 2020;9(11):30, https://doi.org/10.1167/tvst.9.11.30

Purpose: To establish a method of laser capture microdissection (LCM) and RNA microsequencing for exploring optic nerve crush (ONC)–related early mRNA alterations in retinal ganglion cell (RGC) layer.

Methods: An LCM protocol was developed using retinal tissue sections to obtain high-quality RNA for microsequencing. Cells in the RGC layer were collected by laser pressure catapulting (LPC) using a PALM Zeiss UV LCM system. The effect of section thickness and slide type on tissue capture success and RNA yield and the integrity after LCM were evaluated. The optimal LCM protocol was used to explore ONC-related early mRNA alterations in the RGC layer. Candidate genes were validated by real-time polymerase chain reaction of the RGC layer tissue dissected by "cut and LPC" using the same LCM system.

Results: We successfully established an optimal LCM protocol using 30-µm–thick retinal tissue sections mounted on glass slides and laser pressure catapulting (LPC) to collect cells in the RGC layer and to obtain high-quality RNA for microsequencing. On the basis of our protocol, we identified 8744 differentially expressed genes that were involved in ONC-related early mRNA alterations in the RGC layer. Candidate genes included Atf3, Lgals3, LOC102551701, Plaur, Tmem140, and Maml1.

Conclusions: The LCM-based single-cell RNA sequencing allowed a new sight into the early mRNA changes of RGCs highlighting new molecules associated to ONC.

Translational Relevance: This technique will be helpful for more accurate transcriptome analysis of clinical pathological samples of ophthalmology and provide important reference for the discovery of new pathological diagnosis indicators and drug development targets.

Introduction

Retinal ganglion cell (RGC) death and axonal degeneration are common processes in optic nerve diseases, such as traumatic optic neuropathy and glaucoma. The optic nerve crush (ONC) model has proven useful for the study of RGC survival or death. RGC death commences within five to six days after ONC injury, with more than 90% RGC loss after 14 days.[1] ONC-related mRNA changes have been documented in cell and animal models. However, RNA profiling studies focusing on early changes in the RGC layer after ONC are still rare.

Laser capture microdissection (LCM) allows the isolation of specific cell populations from complex tissues that can then be used for gene expression studies.[1] Microsequencing using single-cell RNA sequencing (scRNA-seq) technique can amplify a small amount of RNA (from at least one cell, approximately 10 pg) at the ng level to obtain the amount of nucleic acid needed for high-throughput sequencing. Although studies involving 10× scRNA-seq of the retina have been reported recently,[2,3] and their results have been valuable, there are still some shortcomings. This technique does not distinguish cells in advance; therefore there is a large amount of sequencing data that cannot be referenced to target cells, which is not economical. In addition, no pathological sections are used as a reference, and it is unknown whether the samples are representative of the disease. Therefore it may be of great significance to establish a more economical RNA microsequencing method, especially for abnormal cells in pathological sections.

In the present study, we adopted an optimal protocol combined with LCM and RNA microsequencing to examine the early changes in the RGC layer RNA profile in an ONC model. Our results also revealed ONC-related early mRNA alterations in RGC layer and identified several candidate genes for further studies.

Materials and Methods

Workflow Used for Laser Capture Microdissection and RNA Microsequencing

Our protocol was divided into two parts: optimization of the LCM protocol and determination of the ONC-related early mRNA alterations in RGC layer.

In part one, enucleated eyes were prepared for sectioning. Glass slides and polyethylene naphthalate (PEN) membrane-coated slides were used, and tissue sections with a thickness of 20 µm or 30 µm were used. Three slides obtained from three rats for each group were analyzed The effects of section thickness and slide type on the tissue capture success and RNA quality after LPC using the PALM Zeiss UV LCM system were analyzed (Figs. 1A and 1C).

In part two, the optimized LCM protocol was used to explore ONC-related early mRNA alterations in RGC layer. Three rats were used in each group. Cells in RGC layer were captured from three slides obtained from ONC eyes or control eyes. Candidate genes were validated by real-time polymerase chain reaction (RT-PCR) of RGC layer tissue dissected by the "cut and LPC" method using the same LCM system describe above. (Figs. 1B and 1D) Three samples from three rats were used at each time point.

Animals and ONC Model

Adult (150–200 g) male Wistar rats were included in the present study. The animals were housed in conditions with a constant room temperature (21°–22°C) and a 12-hour light/12-hour dark cycle and given free access to food and water. All experiments were performed according to the Guidance for the Care and Use of Laboratory Animals recommended by the National Institutes of Health, ARVO Animal Statement and were approved by the Ethics Committee for Animal Experimentation of the Second Military Medical University.

To establish the ONC model, the rats were intraperitoneally anesthetized with 10% chloralhydrate (4 mL/kg), and intraorbital ONC was performed in the left eye as previously described.[4] Briefly, the optic nerve was surgically exposed under the superior orbital margin and crushed using an aneurysm clip (mini clip, temporary; Aesculap, Tuttlingen, Germany) 2 mm posterior to the lamina cribrosa for 8 seconds without damaging any small vessels. Sham surgery was performed in the right eye. Animals were sacrificed and perfused intracardially with phosphate-buffered saline solution (PBS) on day 3 after crush.

Tissue Preparation

Eyes were removed corneas and lens and then embedded using optimal cutting temperature embedding medium (Sakura Tissue-Tek O.C.T. Compound; Sakura Finetek USA, Inc., Torrance, CA, USA) by rapid freezing under crushed dry ice and stored at −80°C.

Glass slides and PEN membrane-coated slides were disinfected with ultraviolet light, and the tissues were sectioned with a CM1950 cryostat microtome (Leica

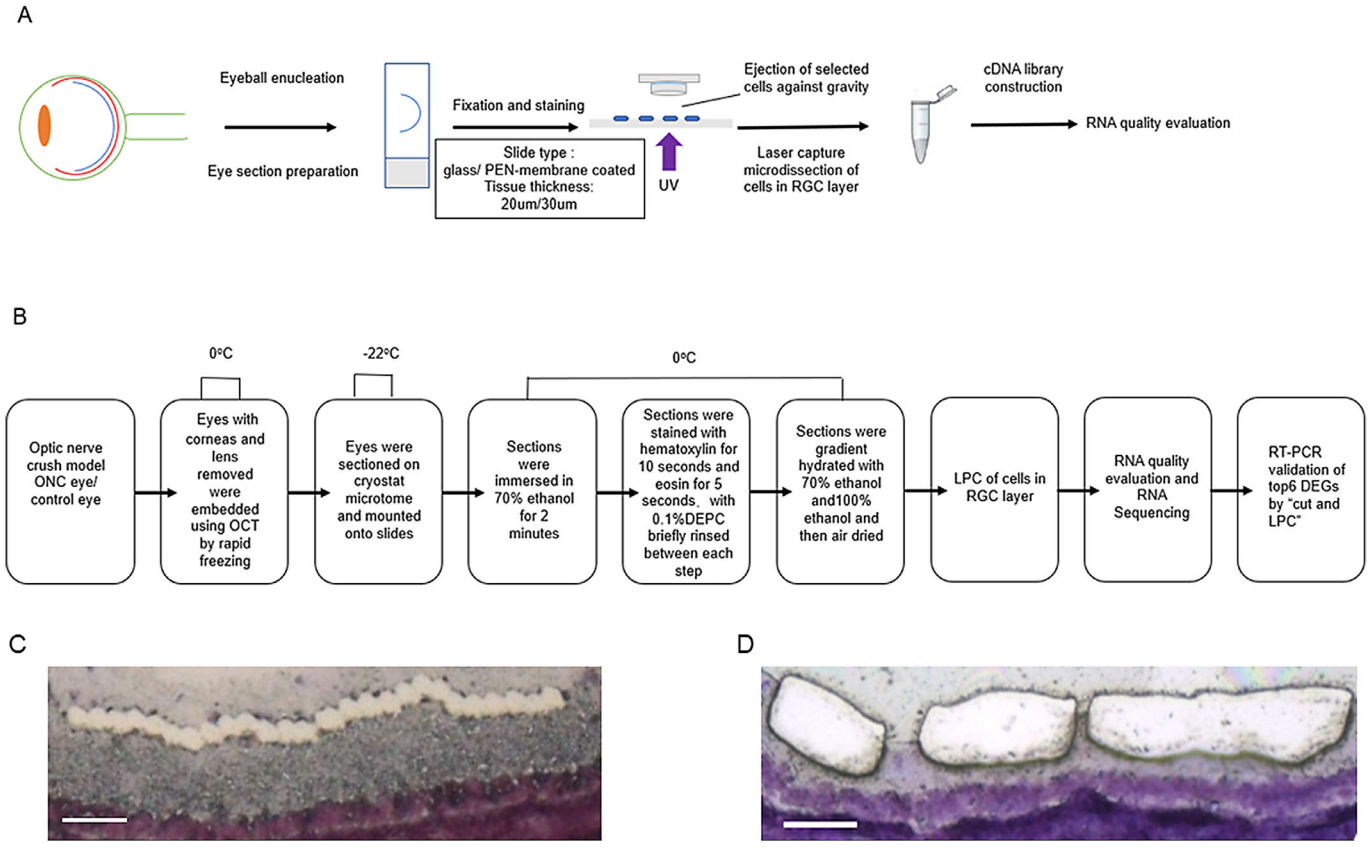

Figure 1. Workflow of laser capture microdissection-based sequencing. (**A**) Workflow of optimizing the LCM protocol. (**B**) Workflow of the study of early mRNA alterations in RGC layer after ONC. (**C**) LPC of cells in RGC layer for mRNA sequencing (*scale bar*: 50 µm). (**D**) "Cut and LPC" method for RGC layer for RT-PCR (*scale bar*: 50 µm)

Microsystems Inc, Bannockburn, IL, USA; http://www.leica-microsystems.com) at −22°C at a thickness of 20 µm or 30 µm.

Fixation and Staining

The frozen sections were thawed at room temperature for two minutes and immersed immediately in 70% ethanol for two minutes. After fixation, the slides were rinsed briefly in 0.1% diethyl pyrocarbonate (DEPC) and subjected to hematoxylin and eosin staining with hematoxylin for 10 seconds and eosin for five seconds, with brief rinsing with 0.1% DEPC between each step. The sections were hydrated with a gradient of 70% and 100% ethanol and then air dried. All processes were performed on ice, and all reagents were prepared in 0.1% DEPC.

Laser Capture Microdissection

Cells in the RGC layer with a large round or oval nuclei were microdissected by laser pressure catapulting (LPC) using a Palm Zeiss UV laser capture microdissection system (Palm Zeiss Microlaser Technologies, Munich, Germany) consisting of an inverted microscope with a motorized stage, an ultraviolet (UV) laser and an X-Cite 120 fluorescence illuminator (EXFO). The microdissection process was visualized with an AxioCam ICc camera coupled to a computer and was controlled by Palm RoboSoftware (Zeiss, Germany). Approximately 50 selected cells were ejected against gravity into the cap of an Eppendorf tube filled with 20 µL RNA extraction lysis buffer.

RNA Sequencing and Gene Ontology and Pathway Enrichment Analysis

cDNA libraries were generated from the RNA samples purified from these cells using the Smart-seq2 protocol. One microliter of sample was used to determine the concentration (Qubit 3.0 fluorometer) and integrity (Agilent 2100 Bioanalyzer, Agilent High Sensitivity DNA Kit; Agilent Technologies, Santa Clara, CA, USA). RNA sequencing was performed using the PE100 strategy (HiSeq 2500; Illumina,

San Diego, CA, USA). Sequencing data were then analyzed. Gene expression was quantified according to RPKM (reads per kilobase per million). Comparison of the differential expression genes (DEGs) of mRNAs from ONC and control was performed after normalization of the raw data and application of DESeq2. Genes with a fold change ≥ 2 and a q value < 0.05 were chosen. To analyze the biological classification of the DEGs, gene ontology (GO) and The Kyoto Encyclopedia of Genes and Genomes (KEGG) pathway enrichment analyses were performed using DAVID. $P < 0.01$ was used as the threshold value. The candidate genes were chosen from among DEGs with a $|\log_2 FC| \geq 10$.

cDNA Synthesis and Real-Time Polymerase Chain Reaction (RT-PCR)

Total RNA was isolated from the RGC layer tissue by the "cut and LPC" method using a PALM Zeiss UV laser capture microdissection system and an RNeasy kit (Qiagen, Valencia, CA, USA), and a portion (1 ng) of the RNA were subjected to reverse transcription (RT) with a SMARTer PCR cDNA Synthesis Kit (Clontech, Mountain View, CA, USA). Then, RT-PCR analysis was performed using the TB Green Premix Ex Taq Tli RNaseH Plus kit (Takara, Mountain View, CA, USA). The gene-specific primer sequences were as follows: for Atf3, forward 5′- TCAGTGACAGGGCAGGAAGA −3′, reverse 5′-CCCACAGTGCAGACACCTTC −3′; for Lgals3, forward 5′-TGCCCTACGATATGCCCTTG −3′, reverse 5′- TGAAGCGGGGGTTAAAGTGG-3′; for LOC102551701, forward 5′-AACCCGAT TGTGTGTTTGCG-′, reverse 5′- TTCTGTGATCGT GCTGTGCT-3′; for Plaur, forward 5′-GCGGCCGCGAAGAACC-3′, reverse 5′- C TTCCCATTCCCGAAGCACC-3′; for Tmem140, forward 5′-ATGGGATGGCAAGGGTTCAG-3′, reverse 5′- TGGGTTCCTTGACACCACAG-3′; for Maml1, forward 5′-CGGACATCTCCATGATCCA GT-3′, reverse 5′- GAAGCAGGAGGAAGCCCATT-3′.

Immunohistochemistry

Rats were sacrificed and perfused intracardially with 4% paraformaldehyde (PFA) in PBS. The eyes were removed and immersed in 4% PFA in PBS for 24 hours at 4°C and then in 10%, 20%, and 30% sucrose solution in PBS for 24 hours at 4°C and embedded using optimal cutting temperature embedding medium (Sakura Tissue-Tek O.C.T. Compound) by rapid freezing under crushed dry ice, after which they were stored at −80°C. After embedding, the eyes were sectioned with a CM1950 cryostat microtome (Leica Microsystems Inc, Bannockburn, IL, USA) at −22°C at a thickness of 15 mm. The parasagittal eye sections were stored at 22°C before immunocytochemistry, and eye sections with a visible optic nerve head were chosen.

Tissues were washed in PBS (3 × 5 minutes) and then incubated in blocking solution (5% donkey serum, 0.5% Triton X-100, and 1% bovine serum albumin in PBS) for one hour at room temperature (RT), followed by incubation with primary antibodies overnight at 4°C. The primary antibodies used were rabbit anti-Atf3 (1:500; Abcam, Cambridge, United Kingdom) and rabbit anti-Maml1 (1:500; Abcam). The next day, tissues were washed in PBS (3 × 5 minutes) and incubated with secondary antibodies conjugated to Alexa Fluor 488 (1:400; goat anti–rabbit; Life Technologies, Carlsbad, CA, USA) or Alexa Fluor 594 (1:400; goat anti–rabbit; Life Technologies) for one hour at RT. Retinas were incubated with the nuclear dye DAPI for 20 minutes and washed in PBS (3 × 5 minutes) before microscopic analysis. All sections were observed under a fluorescence microscope (Leica DFC 7000T), and photomicrograph images were captured at magnification × 200.

Statistical Analysis

Continuous variables were compared using the *t* test after the normal distribution test. Categorical variables were compared using χ^2 analysis. Ranked variables were compared using non-parametric tests along with the Mann-Whitney U test. Differences were considered statistically significant when $P \leq 0.05$.

Results

Effect of Section Thickness and Slide Type on Tissue Capture Success, RNA Yield, and Integrity After LCM

Retinal sections with two different thicknesses (20 or 30 µm) that were mounted onto two different types of slides (glass or PEN-membrane coated) were used to determine the best tissue preparation conditions for LCM. The capture success was calculated by dividing the dissected cell number (after the LCM process) by the selected cell number (before the LCM process). Both the 20-µm–thick and 30-µm–thick sections mounted on PEN membrane-coated slides led to poor capture success (16% vs. 20%, $P > 0.05$) since no more than 20% of the selected cells were dissected. And sections mounted on glass slides showed

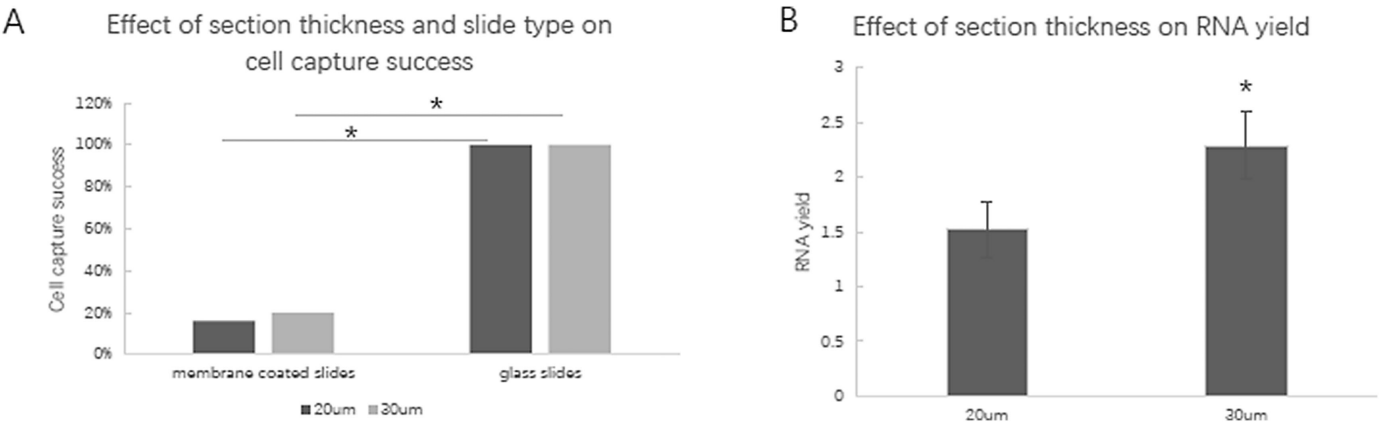

Figure 2. Effect of section thickness and slide type on cell capture success, RNA yield, and integrity after LCM. (**A**) Effect of section thickness and slide type on cell capture success. Both 20-µm–thick and 30-µm–thick sections mounted on PEN membrane-coated slides led to poor capture success (16% vs. 20%, $P > 0.05$). Sections mounted on glass slides led to good capture success (both 100%). (**B**) Effect of section thickness on RNA yield. Twenty-micrometer–thick sections showed a yield of 1.52 ± 0.25 ng/µL, and 30-µm–thick sections showed a yield of 2.29 ± 0.31 ng/µL ($P < 0.05$).

good capture success (both 100%). Regarding the RNA integrity, all the samples from 30 µm-thick sections on glass slides met the demands for library construction, while only 75% of the samples from 20-µm–thick sections were acceptable ($P > 0.05$). Regarding the RNA yield, the 20-µm–thick sections showed a yield of 1.52 ± 0.25 ng/µL, and the 30-µm–thick sections showed a yield of 2.29 ± 0.31 ng/µL ($P < 0.05$, Figs. 2A and 2B). These results showed that PEN membrane–coated slides did not lead to good cell capture. Thirty-micrometer–thick glass sections had higher RNA yield than 20-µm–thick glass sections, with both samples resulting in good RNA integrity for further RNA sequencing analysis.

RNA Sequencing Analysis and Identification of Differentially Expressed Genes (DEGs) Three Days After Crush

The RNA from dissected cells was then amplified and used to generate cDNA libraries using the Smart-seq2 protocol. After RNA sequencing using the PE100 strategy (HiSeq 2500; Illumina), the dissected cells were identified by cell markers. RGC markers such as Pou4 (Brn3), Rbpms, and Slc17ab were shown to be expressed with high FPKM values (Fig. 3B). Astroglial markers such as S100, GFAP, MAP2, and ALDH1L1 were shown to be expressed with low FPKM values. The horizontal cell marker 8A-1, microglia marker

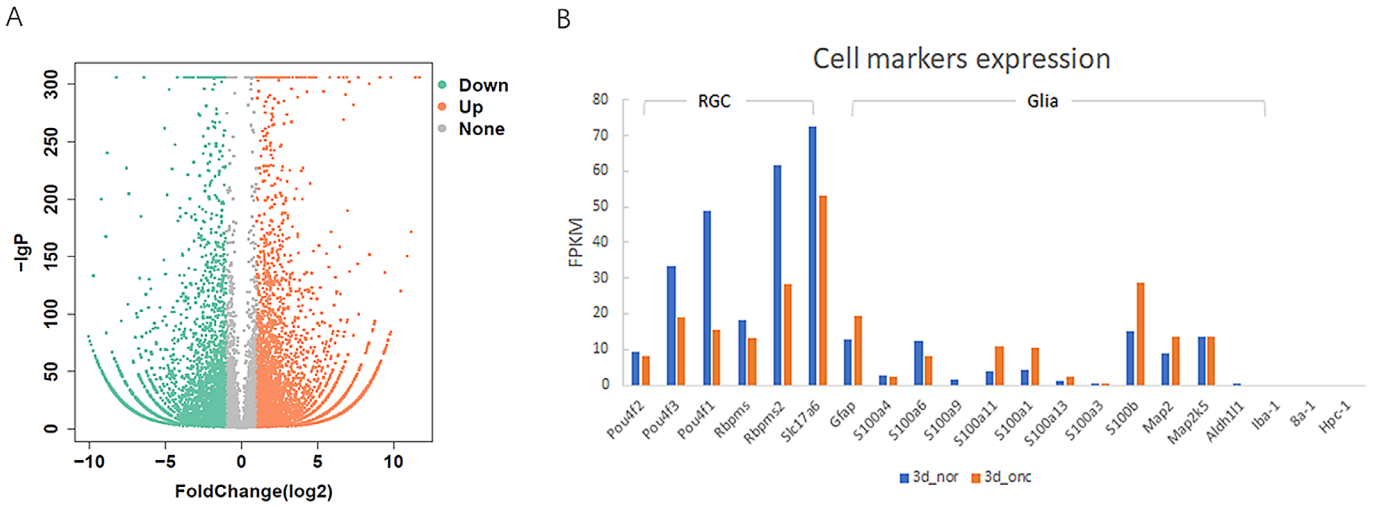

Figure 3. Analysis of scRNA-seq results. (**A**) Volcano plot of DEGs between ONC and control samples. Genes with a fold change ≥ 2 and a q value < 0.05 were chosen. A total of 8744 DEGs were included, with 4411 upregulated genes and 4333 downregulated genes. (**B**) Biomarkers of RGC layer cells. Both RGC markers and glia markers were identified in our sequencing data.

Table. Differentially Expressed Genes With a |log2Ratio|≥10 in RGCs After ONC

Gene	Log2 Fold Change	Q Value	Up/Down	Gene Name	Full Name
Gene27639	11.70331	0	Up	Atf3	Activating transcription factor 3
Gene29150	11.4495	0	Up	Lgals3	Lectin, galactoside-binding, soluble, 3
Gene35168	11.15631	2.35E-172	Up	LOC102551701	
Gene1274	10.90482	3.32E-151	Up	Plaur	Plasminogen activator, urokinase receptor
Gene10710	10.47381	1.28E-120	Up	Tmem140	Transmembrane protein 140
Gene22509	−10.0667	2.07E-81	Down	Maml1	Mastermind-like 1

Iba-1, and amacrine cell marker HPC-1 were not found in our results.

Comparison of the differential expression profiles of mRNAs from ONC and control was performed. A total of 8744 DEGs were included, with 4411 upregulated genes and 4333 downregulated genes (Fig. 3A, Supplementary Table 1). The candidate genes were chosen from among DEGs with a $|\log_2 FC| \geq 10$, including five genes that were unexpressed and one gene that was downregulated in ONC compared with control (Table).

GO and KEGG Enrichment Analyses of the DEGs

To analyze the biological classification of the DEGs, functional and pathway enrichment analyses were performed using DAVID. The GO analysis results showed that the DEGs related to biological processes (BP) were significantly enriched in multicellular organismal process, single-multicellular organism process, and biological adhesion, etc. (Supplementary Fig. S1). DEGs with changes in molecular function (MF) were mainly enriched in receptor activity, signaling receptor activity, and transmembrane signaling receptor activity, etc. (Supplementary Fig. S2). DEGs with changes in cell components (CC) were mainly enriched in integral components of the plasma membrane, intrinsic components of the plasma membrane, and intrinsic components of the membrane, etc. (Supplementary Fig. S3). An additional functional analysis of mRNAs based on KEGG pathways showed that the neuroactive ligand−receptor interaction pathway was significant changed in ONC versus control.

RT-PCR Gene Expression Analysis

RGC layer was microdissected by the "cut and LPC" method using the PALM MicroBeam system, and the RNA was extracted using a column-based method. Total RNA was subjected to reverse transcription (RT) with a SMARTer PCR cDNA Synthesis Kit and then used for RT-PCR analysis. Atf3(activating transcription factor 3), Lgals3 (lectin, galactoside-binding, soluble, 3), LOC102551701, Plaur (plasminogen activator, urokinase receptor) and Tmem140 (transmembrane protein 140) levels were unregulated in ONC eyes compared to the mRNA levels in the control eyes at one, two, and three days after crush, while the Maml1 (Mastermind-like 1) mRNA level was decreased in the ONC eyes compared to that in the control eyes at one, two, and three days after crush (Fig. 4A).

Immunohistochemistry of Atf3 and Maml1

Retinal immunostaining of the Atf3 and Maml1 proteins confirmed the apparent changes in protein expression after ONC. In the control retinas, there was low Atf3 immunoreactivity and obvious Maml1 immunoreactivity throughout all retinal layers. In the ONC retinas, there was higher Atf3 and lower Maml1 immunoreactivity in the RGC layer (Figs. 4B and 4C).

Discussion

LCM is often used to study the expression of both minimally or abundantly expressed genes in different brain regions[5–9] and occasionally in retinas.[10–12] In our study, we adopted an optimal LCM protocol with microsequencing to examine the early mRNA changes in RGC layer in an optic nerve crush model.

During the LCM process, capture success depends on the tissue section thickness and the slide type. A previous study showed that 10-µm–thick tissue sections were not adequate for the capture of microdissected tissue and that the resulting RNA was totally degraded.[5] In our study, we found that 30-µm–thick tissue sections had high capture success and RNA yield when using the PALM system. However, this might not be applicable to another LCM system, such as the Arcturus LCM system because it possesses a low-energy infrared laser that cannot catapult thicker tissue sections.[13]

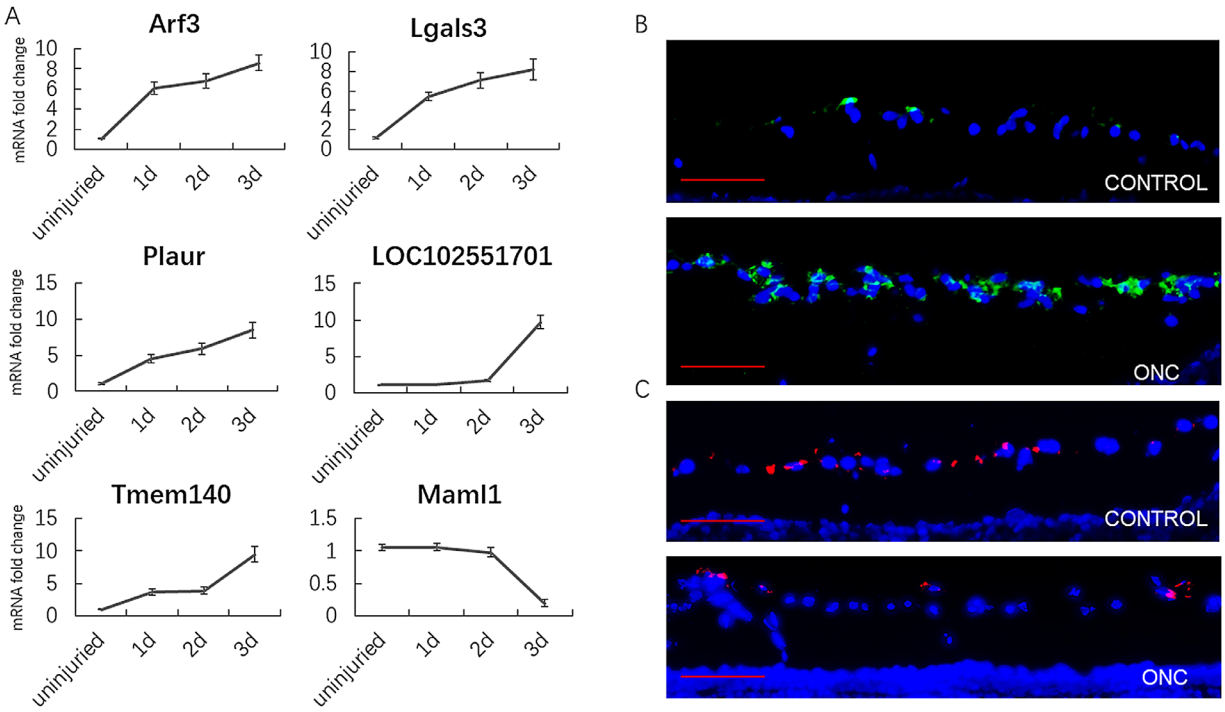

Figure 4. Verification of candidate genes. (A) RT-PCR of DEGs with a |log2Ratio|≥10. Atf3, Lgals3, LOC102551701, Plaur and Tmem140 levels were found to be upregulated, whereas Maml1 mRNA was found to be decreased at one, two, and three days after crush in the ONC eyes compared to the control eyes. (B) Immunohistochemistry of ATF3 three days after crush. In the control retina, there was low Atf3 immunoreactivity, while in the ONC retina, Atf3 expressed at a high level (*green*: ATF3; *blue*: DAPI; *scale bar*: 200 µm). (C) Immunohistochemistry of Maml1 three days after crush. In control retinas, there was high Maml1 immunoreactivity, while in ONC retinas, Maml1 immunoreactivity was low in the RGC layer (*red*: Maml1; *blue*: DAPI; *scale bar*: 200 µm).

It was reported that membrane-coated slides made it possible to capture larger tissue areas with lower laser intensity and time compared with glass slides.[14] However, others reported that tissue sections mounted on glass slides led to higher capture success and RNA yield compared with sections mounted on PEN membrane-coated slides.[5] The increase in adhesion between tissue and PEN-membrane slides made it difficult to catapult the tissue, which was also observed in our study.

There were RGC markers and also glia markers in our sequencing data, which means our results represent a mixed cells in RGC layer. Combined with RGC immunohistochemistry, LCM-based RNA microsequencing might help to identify and collect pure RGCs, which would be more economical compared with currently reported 10× scRNA-seq method for RGCs.

We found a large number of DEGs 3 days after ONC. GO and KEGG enrichment analyses showed DEGs were significantly enriched in receptor activity, which means receptor activity was involved in the early stage after ONC. We chose candidate genes with a $|\log_2 FC| \geq 10$ and found Atf3, Lgals3, LOC102551701, Plaur, Tmem140, and Maml1.

Atf3 was previously found to be significantly changed in ONC RGC layer.[12,15] This was in accord with our results, and it also proved the reliability of our results. Atf3 was reported to be involved in axonal regeneration, because Atf3 expression was activated after crush, and axonal regeneration was enhanced in various types of neurons as a result.[16–18] More recently, Atf3 was reported to protects RGC and promote visual function after ONC.[19] Our results implied that Atf3 and axonal regeneration started in the early stage after ONC.

Lgals3 is a multifunctional protein that participates in mediating inflammatory reactions and cell proliferation, adhesion, migration, and apoptosis. The expression of Lgals3 was reported in astrocytes and microglia induced by neuroinflammation[20,21] and was involved in autophagy in the central nervous system (CNS).[22] The increase in Lgals3 after ONC in our results might be due to its expression by activated astrocytes in the RGC layer.

Plaur, the receptor for the plasminogen activator of the urokinase type (uPAR), is involved in many physiological and pathological processes and participates in the development, function, and pathology of

the central nervous system[23] The uPAR leads to activation of the Rho family small GTPase Rac1 and induced axonal regeneration in the CNS.[24] We also suggest the increased Plaur levels according to our results could lead to Rac1-induced axonal regeneration after ONC, which needs further study.

Another interesting candidate was Maml1. The close correlation of the spatial and temporal expression of Maml1 in the CNS during early development indicates the role of the Maml1 gene in neurogenesis.[25] MAML1 is also a novel modulator of NF-kappa B signaling and regulates cellular survival.[26] Hence, the decrease in Maml1 in the early stage after ONC might reflect the insufficient intrinsic growth state of mature neurons.

There are some limitations of our study. There are some limitations of our study. First, the results were based on microtranscriptome sequencing of a small number of cells, which might not be adequate to reflect the whole RGC layer. Second, because the cells in the RGC layer were undifferentiated captured, our results only reflect the mixed RGC and glia cells in the RGC layer. Further studies and improved protocols are needed to discover the mechanism involved in changes after ONC.

Acknowledgments

The authors thank for Jiajun Xu's critical proofreading of the manuscript.

Supported by the China National Key Research and Development Program Stem Cell and Translational Research Key Projects (2018YFA0108301), National Natural Science Foundation of China (31971109, 31471390), Shanghai Rising-Star Program (17QA1405400) and Shanghai Health and family planning system program (2017YQ028).

Disclosure: **D. Pan,** None; **M. Xu,** None; **X. Chang,** None; **M. Xia,** None; **Y. Fang,** None; **Y. Fu,** None; **W. Shen,** None; **Y. Wang,** None; **X. Sun,** None

* DP, MX, XC, and MX contributed equally to this work.

References

1. Datta S, Malhotra L, Dickerson R, Chaffee S, Sen CK, Roy S. Laser capture microdissection: Big data from small samples. *Histol Histopathol*. 2015;30(11):1255–1269.
2. Tran NM, Shekhar K, Whitney IE, et al. Single-cell profiles of retinal ganglion cells differing in resilience to injury reveal neuroprotective genes. *Neuron*. 2019;104(6):1039–1055.e1012.
3. Peng YR, Shekhar K, Yan W, et al. Molecular classification and comparative taxonomics of foveal and peripheral cells in primate retina. *Cell*. 2019;176(5):1222–1237.e1222.
4. Chen M, Xiang Z, Cai J. The anti-apoptotic and neuro-protective effects of human umbilical cord blood mesenchymal stem cells (hUCB-MSCs) on acute optic nerve injury is transient. *Brain Res*. 2013;1532:63–75.
5. Garrido-Gil P, Fernandez-Rodriguez P, Rodriguez-Pallares J, Labandeira-Garcia JL. Laser capture microdissection protocol for gene expression analysis in the brain. *Histochem Cell Biol*. 2017;148(3):299–311.
6. Corgiat BA, Mueller C. Using laser capture microdissection to isolate cortical laminae in nonhuman primate brain. *Methods Mol Biol*. 2017;1606:115–132.
7. Simpson JE, Wharton SB, Heath PR. Immuno-laser-capture microdissection for the isolation of enriched glial populations from frozen post-mortem human brain. *Methods Mol Biol*. 2018;1723:273–284.
8. Mauney SA, Woo TW, Sonntag KC. Cell type-specific laser capture microdissection for gene expression profiling in the human brain. *Methods Mol Biol*. 2018;1723:203–221.
9. Tagliafierro L, Bonawitz K, Glenn OC, Chiba-Falek O. Gene expression analysis of neurons and astrocytes isolated by laser capture microdissection from frozen human brain tissues. *Front Mol Neurosci*. 2016;9:72.
10. Chung SH, Shen W, Gillies MC. Laser capture microdissection-directed profiling of glycolytic and mTOR pathways in areas of selectively ablated Muller cells in the murine retina. *Invest Ophthalmol Vis Sci*. 2013;54(10):6578–6585.
11. Funke S, Perumal N, Beck S, et al. Glaucoma related proteomic alterations in human retina samples. *Sci Rep*. 2016;6:29759.
12. Ueno S, Yoneshige A, Koriyama Y, Hagiyama M, Shimomura Y, Ito A. Early gene expression profile in retinal ganglion cell layer after optic nerve crush in mice. *Invest Ophthalmol Vis Sci*. 2018;59(1):370–380.
13. Sluka P, O'Donnell L, McLachlan RI, Stanton PG. Application of laser-capture microdissection to analysis of gene expression in the testis. *Progr Histochem Cytochem*. 2008;42(4):173–201.

14. Kummari E, Guo-Ross SX, Eells JB. Laser capture microdissection—A demonstration of the isolation of individual dopamine neurons and the entire ventral tegmental area. *J Vis Exp*. 2015;96: e52336.
15. Saul KE, Koke JR, Garcia DM. Activating transcription factor 3 (ATF3) expression in the neural retina and optic nerve of zebrafish during optic nerve regeneration. *Comp Biochem Physiol A Mol Integr Physiol*. 2010;155(2):172–182.
16. Neve LD, Savage AA, Koke JR, Garcia DM. Activating transcription factor 3 and reactive astrocytes following optic nerve injury in zebrafish. *Comp Biochem Physiol Toxicol Pharmacol*. 2012;155(2):213–218.
17. Seijffers R, Mills CD, Woolf CJ. ATF3 increases the intrinsic growth state of DRG neurons to enhance peripheral nerve regeneration. *J Neurosci*. 2007;27(30):7911–7920.
18. Gey M, Wanner R, Schilling C, Pedro MT, Sinske D, Knoll B. Atf3 mutant mice show reduced axon regeneration and impaired regeneration-associated gene induction after peripheral nerve injury. *Open Biology*. 2016;6(8):160091.
19. Kole C, Brommer B, Nakaya N, et al. Activating transcription factor 3 (ATF3) protects retinal ganglion cells and promotes functional preservation after optic nerve crush. *Invest Ophthalmol Vis Sci*. 2020;61(2):31.
20. Ramirez E, Sanchez-Maldonado C, Mayoral MA, et al. Neuroinflammation induced by the peptide amyloid-beta (25-35) increase the presence of galectin-3 in astrocytes and microglia and impairs spatial memory. *Neuropeptides*. 2019;74:11–23.
21. Siew JJ, Chen HM, Chen HY, et al. Galectin-3 is required for the microglia-mediated brain inflammation in a model of Huntington's disease. *Nat Commun*. 2019;10(1):3473.
22. Mok SW, Riemer C, Madela K, et al. Role of galectin-3 in prion infections of the CNS. *Biochem Biophys Res Commun*. 2007;359(3):672–678.
23. Archinti M, Britto M, Eden G, Furlan F, Murphy R, Degryse B. The urokinase receptor in the central nervous system. *CNS Neurol Disord Drug Targets*. 2011;10(2):271–294.
24. Merino P, Diaz A, Jeanneret V, et al. Urokinase-type plasminogen activator (uPA) binding to the uPA receptor (uPAR) promotes axonal regeneration in the central nervous system. *J Biol Chem*. 2017;292(7):2741–2753.
25. Wu L, Kobayashi K, Sun T, et al. Cloning and functional characterization of the murine mastermind-like 1 (Maml1) gene. *Gene*. 2004;328:153–165.
26. Jin B, Shen H, Lin S, et al. The mastermind-like 1 (MAML1) co-activator regulates constitutive NF-kappaB signaling and cell survival. *J Biol Chem*. 2010;285(19):14356–14365.